*metals*

MDPI

*Review*

# A Critical Review on the Comparative Assessment of Rare-Earth and Non-Rare-Earth Alloying in Magnesium Alloys

**Hafiz Muhammad Rehan Tariq [1,†], Muhammad Ishtiaq [2,†], Hyun-Hak Kang [1], Umer Masood Chaudry [3] and Tea-Sung Jun [1,3,*]**

[1] Department of Mechanical Engineering, Incheon National University, Incheon 22012, Republic of Korea; 202221057@inu.ac.kr (H.M.R.T.)
[2] Department of Materials Engineering and Convergence Technology, Gyeongsang National University, Jinju 52828, Republic of Korea; ishtiaq145@gnu.ac.kr
[3] Research Institute for Engineering and Technology, Incheon National University, Incheon 22012, Republic of Korea
* Correspondence: t.jun@inu.ac.kr
† These authors contributed equally to this work.

**Abstract:** Magnesium (Mg) alloys have emerged as highly sought-after alloys in aerospace, automotive, and biomedical engineering industries due to their low density and excellent mechanical properties. The addition of alloying elements plays a critical role in improving the performance of these Mg alloys, with rare-earth (RE) elements being especially helpful in improving mechanical properties, specifically strength and ductility. However, due to the higher cost and limited availability of RE elements, researchers are trying to explore non-rare-earth (non-RE) alternatives, such as aluminum, calcium, zinc, etc. These non-RE elements offer various advantages including cost effectiveness and enhanced manufacturability, but they may not always match the performance improvements of RE elements. This review critically examines and compares the effects of RE and non-RE alloying elements on the microstructural evolution, corrosion resistance, and strengthening implications of Mg alloys. Furthermore, it explores the recent advancements in alloy development and evaluates the trade-offs between RE and non-RE alloying elements, offering key insights into the optimal approaches for enhancing the performance of Mg alloys across various applications.

**Keywords:** rare earth; non-rare earth; Mg alloys; precipitation hardening; texture weakening

check for updates

Academic Editor: Rebecca L. Higginson

Received: 6 January 2025
Revised: 22 January 2025
Accepted: 24 January 2025
Published: 27 January 2025

**Citation:** Tariq, H.M.R.; Ishtiaq, M.; Kang, H.-H.; Chaudry, U.M.; Jun, T.-S. A Critical Review on the Comparative Assessment of Rare-Earth and Non-Rare-Earth Alloying in Magnesium Alloys. *Metals* **2025**, *15*, 128. https://doi.org/10.3390/met15020128

**Copyright:** © 2025 by the authors. Licensee MDPI, Basel, Switzerland. This article is an open access article distributed under the terms and conditions of the Creative Commons Attribution (CC BY) license (https://creativecommons.org/licenses/by/4.0/).

## 1. Introduction

The increasing global emphasis on stringent emission regulations, particularly in developed countries, has heightened the demand for lightweight, high-strength materials to enhance fuel efficiency and reduce environmental impact [1,2]. In response, researchers worldwide are actively pursuing the development of such materials. Among structural metals, magnesium (Mg) stands out due to its exceptionally low density, making it a prime candidate for automotive and structural applications where weight reduction is critical [3]. Despite its advantages, the widespread use of Mg is hindered by its inherently low strength [4,5]. To address this limitation, significant efforts have been directed toward developing Mg alloys with enhanced mechanical properties [6–8]. Various alloying elements are incorporated into Mg, leveraging diverse strengthening mechanisms such as grain refinement [9,10], precipitation strengthening [11,12], dispersion strengthening [13], and texture hardening [14,15]. These alloying strategies can be broadly classified into two

categories: (i) rare-earth (RE) Mg alloys [16] and (ii) non-rare-earth Mg alloys [17]. Each category offers distinct advantages and challenges, providing a wide scope for tailoring Mg alloys to meet specific performance requirements for advanced engineering applications.

There is an extensive body of literature on Mg alloys, including several review articles that primarily focus on their development and applications [18,19]. Much of the research centers on alloying strategies, particularly the addition of alloying elements to improve properties such as extrudability and strength [20–22]. Numerous studies have reported on the deformation mechanisms of these alloys [23], mechanical properties [24], and grain refinement strategies [25] and substantial data are available on their corrosion behavior [26,27]. Additionally, many investigations focus on applications in the biomedical field [28,29], with biocompatibility being a key consideration [30]. There are some reviews that only focus on the research related to a particular country [23,31]. Some reviews specifically address RE-based Mg alloys [32–34], while others focus on non-RE-based Mg alloys [35]. However, there remains a lack of a comprehensive and concise review that simultaneously discusses the effects of both RE- and non-RE-based Mg alloys. This review aims to fill this gap by providing an integrated overview of recent advancements in both RE- and non-RE-based Mg alloys, highlighting their composition, microstructural evolution, texture development, strengthening implications, and corrosion resistance. By sharing this knowledge, the review seeks to offer the research community a holistic understanding of Mg alloys with diverse compositions and properties.

## 2. Microstructural Variations Induced by RE and Non-RE Alloying Elements

Rare-earth (RE) alloying in magnesium (Mg) alloys is well known for its significant grain refinement capabilities [25]. Elements such as gadolinium (Gd) [36], yttrium (Y) [37,38], neodymium (Nd) [39], lanthanum (La) [40], and cerium (Ce) [41] have proven to be particularly effective in improving strength through grain refinement, as explained by the Hall–Petch relationship [42]. Refinement is attributed to the conventional super-cooling effect that occurs at the liquid/solid interface during solidification due to the segregation of RE solutes [43]. This super-cooling effect enhances the nucleation of new grains, effectively limiting the growth of existing grains when the undercooling conditions necessary for the most effective nucleating particles are met. Additionally, RE-containing intermetallic phases observed at grain boundaries support this mechanism by stabilizing the refined grain structure [44].

A useful parameter for evaluating the grain refinement potential of different RE elements is the growth restriction factor (GRF), defined by the relation between the liquidus line slope and the coefficient of solute partition with constant concentration [45]. Higher GRF values correlate with stronger grain refinement. Studies have indicated that Nd exhibits a particularly strong effect on restricting the growth of $\alpha$-Mg grains, surpassing many other RE elements [46]. Although the refinement effect is significantly enhanced with increasing RE content, it eventually approaches saturation, yielding negligible incremental improvement as GRF levels continue to rise. Besides rare-earth elements, zirconium (Zr) [47] and Zn [48] are frequently used as alloying agents in WE-series Mg alloys. Zn, in particular, stands out as the most effective grain refiner for magnesium alloys, contributing to notable enhancements in structural consistency. This uniform microstructure results in improved overall properties of the alloy. Zr is typically added via commercial Mg-Zr master alloys, which, based on the Mg-Zr binary phase diagram, have limited solid solubility in liquid Mg of approximately 0.44 wt.% [49]. This constraint results in Zr existing as both undissolved particles and dissolved solutes. Each type of Zr influences grain refining through a distinct method. The presence of Zr solutes causes strong constitutional super-

cooling that restricts the growth of α-Mg dendrites [50]. The undissolved Zr particles also aid in intermetallic transition and heterogeneous nucleation. Notably, the Q value for Zr solutes, calculated at around 38.3 °C for a Zr content of 1 wt.%, is significantly higher than that of typical RE elements, suggesting a superior grain refinement potential [51]. However, the efficiency of Zr in Mg-RE alloys varies between its solute and particulate forms. Solute Zr is more effective in refining grains compared to Zr particles. A challenge with commercial Mg-Zr master alloys is that they often contain clusters of Zr particles, which can precipitate and settle in liquid Mg, reducing their effectiveness over time [52].

To overcome these challenges, new grain refiners such as Al have emerged as a promising option due to their affordability and strong refining effects. The mechanism of Al refinement involves in situ reactions with RE elements to form $Al_2RE$ particles, which reduce interfacial energy with α-Mg and serve as heterogeneous nucleation sites [53]. The composition, content, and distribution of these second phases vary based on the specific RE elements and Mg-RE alloy types, affecting the overall refinement effectiveness [32]. For instance, in Mg-Nd alloys refined with Al, a needle-like $Al_{11}Nd_3$ phase forms as Al content increases, with the optimal refinement effect achieved at over 2% Al when $Al_2Nd$ phases begin to appear [54]. Conversely, in Mg-Y alloys, a smaller Al content of less than 1% yields the best refinement, forming only the $Al_2Y$ phase. The effectiveness of Al as a refiner is also influenced by the specific combination and concentration of RE elements in multi-component Mg-RE alloys commonly used in industry [55]. For example, research by Liu et al. [56] demonstrated that the Gd and Y contents in Mg-Gd-Y-Al alloys significantly affect phase composition and refinement outcomes, although the underlying mechanisms require further investigation.

In Figure 1a, the Mg-Y alloy without refinement displays a coarse dendritic structure, with an average grain size of 694.3 μm. As shown in Figure 1b, adding Al to the Mg-Y alloy leads to substantial grain refinement, transforming the dendritic morphology into equiaxed grains and reducing the average grain size to 73.2 μm [57]. Similarly, the introduction of Zr, as illustrated in Figure 1c, also refines the grain structure of the Mg–Y alloy, achieving an average grain size of 71.6 μm [58]. The grain refinement effects of Al and Zr are thus comparable. Moreover, the optical microstructures of the as-cast GWZ alloys, shown in Figure 1d, reveal a clear dendritic morphology across the samples. Among the alloys examined, the GZ141M alloy (Mg-2.5Gd-0.5Zn-0.4Mn) demonstrates the smallest grain size, attributed to its low Y/Gd ratio. As the Y/Gd ratio increases in alloys like GWZ1021M (Mg-1.75Gd-0.75Y-0.5Zn-0.4Mn) and GWZ741M (Mg-1.25Gd-1.25Y-0.5Zn-0.4Mn), grain size increases correspondingly, suggesting that Gd is more effective than Y in promoting grain refinement in as-cast conditions. Additionally, comparing the GZ141M, GWZ1021M, and GWZ1421M (Mg-2.5Gd-0.75Y-0.5Zn-0.4Mn) alloys (Figure 1a,b,d) reveals that individual additions of either Y or Gd lead to reduced grain sizes in the GZ141M and GWZ1021M alloys, in contrast to the GWZ1421M alloy [57].

Ca stands out among alloying elements in Mg alloys for its ability to significantly enhance fine grain structure and drive the formation of secondary phases within Mg–Zn-RE systems [59]. Figure 1h,i illustrate the microstructure of two extruded Mg-Zn-Nd alloys, with and without Ca addition. The addition of Ca significantly refines the grain structure, reducing the average grain size from approximately 10 μm in the ZNd10 alloy to about 5 μm in the ZXNd100 alloy. Here, the addition of Ca to the Mg-Zn-Nd alloy promotes the formation of nanosized $Mg_2Ca$ and $Zn_3Nd$ particles. The presence of $Mg_2Ca$ particles acts as heterogeneous nucleation sites, enhancing the grain refinement process. During recrystallization, these particles create a strong pinning effect on the grain boundaries, which hinders their movement and prevents grain coarsening. Additionally, the joint

precipitation of $Mg_2Ca$ and $Zn_3Nd$ nanoparticles, with their coherent interface with the Mg matrix, promotes stability within the microstructure [46].

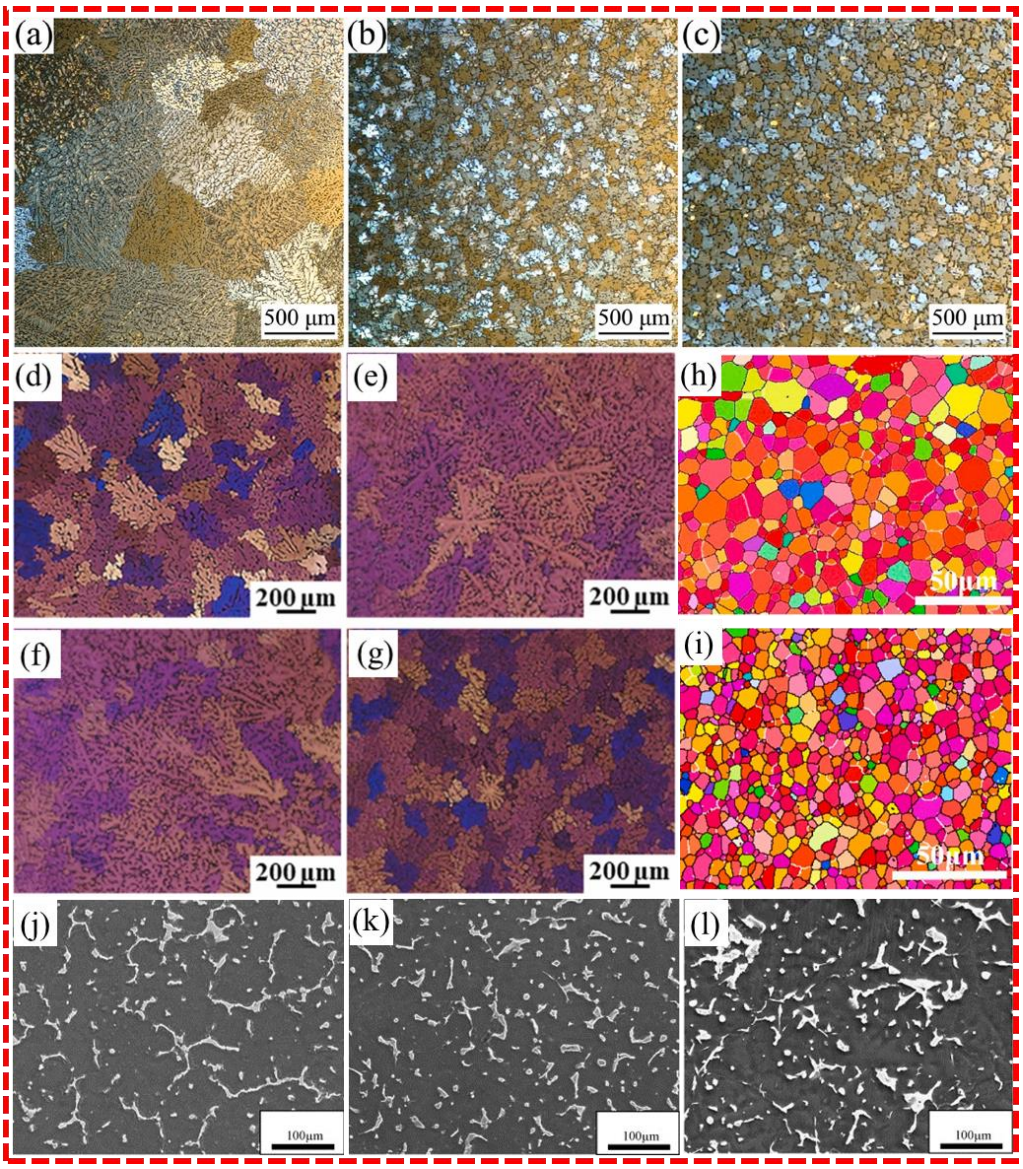



**Figure 1.** Effect of RE alloying on microstructure variation and precipitate formation; optical micrographs of (**a**) Mg-Y alloy, (**b**) Mg-Y-Al alloy, (**c**) Mg-Y-Zr alloy, (**d**) GZ141M alloy, (**e**) GWZ1021M alloy, (**f**) GWZ741M alloy, and (**g**) GWZ1421M alloy; EBSD IPF maps of (**h**) ZNd10 alloy and (**i**) ZXNd100 alloy; and SEM images of (**j**) ZA84-0.5RE alloy, (**k**) ZA84-1.0RE alloy, and (**l**) ZA84-1.5RE alloy (Reprinted from [46,57–59]).

Wang et al. [60] studied the effects of RE additions on the microstructural evolution of the Mg-8Zn-4Al (ZA84) alloy and found that in the absence of RE, the ZA84 alloy exhibits a quasi-continuous network of τ phases and isolated $\varphi$ phases to form a coarse dendritic structure (Figure 1j). Upon introducing 1.0 wt.% RE, the microstructure undergoes significant transformation, with the networked $\tau$ phases breaking into discontinuous, particle-like, or short-bar shapes (Figure 1k). Additionally, a small fraction of block-shaped phases ($Mg_3Al_4Zn_2RE$) appears, reflecting the influence of RE in modifying the phase morphology and distribution. When the RE content is increased to 1.5 wt.%, the formation of $Mg_3Al_4Zn_2RE$ phases becomes more pronounced, indicating that higher RE concentrations promote the generation of these block-shaped phases. This microstructural refinement

contributes to a uniform distribution of phases and reduced grain size, as illustrated by the relationship between RE content and grain boundaries [60]. However, the high density of RE elements and their high cost make this technique unfeasible for industrial-scale applications, hence impeding the widespread usage of RE alloying in large-scale Mg components [23].

Alloying with non-RE elements is subsequently being investigated in order to preserve cost effectiveness and scalability while achieving the required structure–property relationship. Al, Ca, Mn, and Zn are among the most widely utilized non-RE elements for alloying Mg to achieve superior properties through precipitation strengthening and grain refinement [61–63]. These alloying additions result in precipitates with varying sizes, shapes, and morphologies, which significantly influence the microstructure and texture of Mg alloys. The precipitates formed by these non-RE elements nucleate slowly during aging and are distributed unevenly, potentially causing variations in grain size across different regions of the samples. For example, the microstructure of AZ61 Mg alloys has been demonstrated to be significantly impacted by the addition of CaO. Figure 2a–g show the OM, SEM, and TEM images where the AZ61 alloy is primarily composed of coarse grains; however, clusters of smaller grains were observed when 0.5 wt.% and 1 wt.% CaO were added. Additionally, the visible second-phase particles in SEM images were increased from 1.1% in the AZ61 alloy to 2.4% and 7.8% in the AZ61-0.5CaO and AZ61-1CaO alloys, respectively. An EDS analysis indicates that these second-phase particles are composed of Mg, Al, and Ca mostly, which suggest the existence of the $(Mg, Al)_2Ca$ Laves phase in addition to the $Mg_{17}Al_{12}$ phase. These particles serve as the nucleation sites for dynamic recrystallization (DRX) during thermomechanical processes and facilitate the growth of refined grain clusters [64].

Another study reported the formation of $Mg_6Zn_3Ca_2$ precipitates with varying sizes and shapes due to the combined addition of Zn and Ca in the Mg alloy (Figure 3a) [65]. Li et al. conducted a detailed analysis of the 3D atom map of Mg, Ca, and Zn in a 0.3 h-aged Mg-Ca-Zn alloy sample, demonstrating the enrichment of Ca and Zn within densely dispersed plates at a number density of approximately $1.2 \times 10^{24}$ $m^{-3}$ (Figure 3b). Notably, these elements exhibit a propensity to segregate along the basal planes, forming ordered Guinier–Preston [49] zones [66]. G-P zones are essential for altering the microstructure as they act as precipitate nucleation sites. On particular crystallographic planes, these atomically organized, coherent zones develop, introducing fine-scale characteristics that refine the microstructure. Their interaction with the Mg matrix changes the behavior of grain boundaries, enhances DRX, and affects the distribution of precipitates [67]. For instance, Ca atoms can segregate and form clusters, eventually leading to the development of plate-like G-P zones [68], as confirmed by an atom probe tomography (APT) analysis shown in Figure 3c. However, the limited solubility of Ca in Mg leads to more $Mg_2Ca$ precipitates, which are brittle in nature, causing stress concentrations within the microstructure. Controlling the Ca/Al ratio is essential to dictate the microstructure and dominance of intermetallic compounds. The effect of different Al contents in the AZX Mg alloy on precipitate formation and distribution as well as microstructural alterations was recently documented by Tariq et al. [69]. They reported a higher area fraction of Mg-Al-Ca intermetallic compounds in AZX311 due to increased Al content. Here, smaller intermetallic spacing (0.1 μm in AZX311 vs. 0.8 μm in AZX211) was observed, indicating a refined microstructure that enhances grain boundary pinning and impedes dislocation motion (Figure 3d). Li et al. investigated the precipitation behavior in a rolled Mg-3Al-1Ca-1Mn alloy and its impact on microstructure and mechanical properties. Using APT (as shown in Figure 3e), they identified nanoscale $Al_8Mn_5$ particles (~10 nm thick, 40 nm long) with localized Ca segregation, likely formed via dynamic precipitation during rolling.

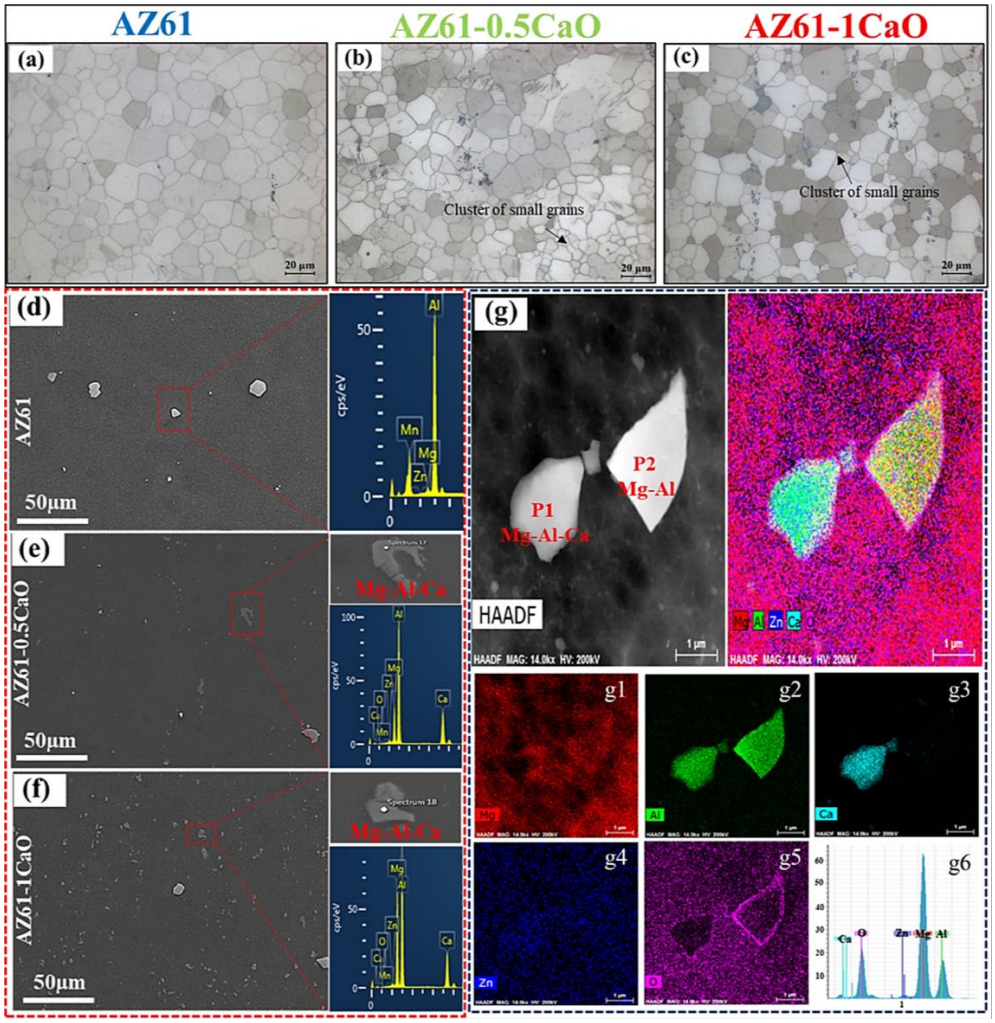



**Figure 2.** Microstructures of Mg alloys; optical micrograph of (**a**) AZ61, (**b**) AZ61-0.5CaO, and (**c**) AZ61-1CaO. SEM images with EDS point analysis of (**d**) AZ61, (**e**) AZ61-0.5CaO, and (**f**) AZ61-1CaO. (**g**–**g6**) HAADF-EDS mapping of AZ61-1CaO alloy showing Mg-Al and Mg-Al-Ca precipitates (reprinted from [64]).

Clusters consisting of Al were also observed within the Mg matrix, while no Ca segregation was detected around micro-$Al_8Mn_5$ or -$Al_3Mn_6$ phases. These findings suggest that dynamic precipitation enhances dynamic recrystallization through particle-stimulated nucleation (PSN), contributing to grain refinement without significant texture changes. The next section will cover the impacts of RE and non-RE alloying elements on the evolution and development of texture in Mg alloys that will be compared.

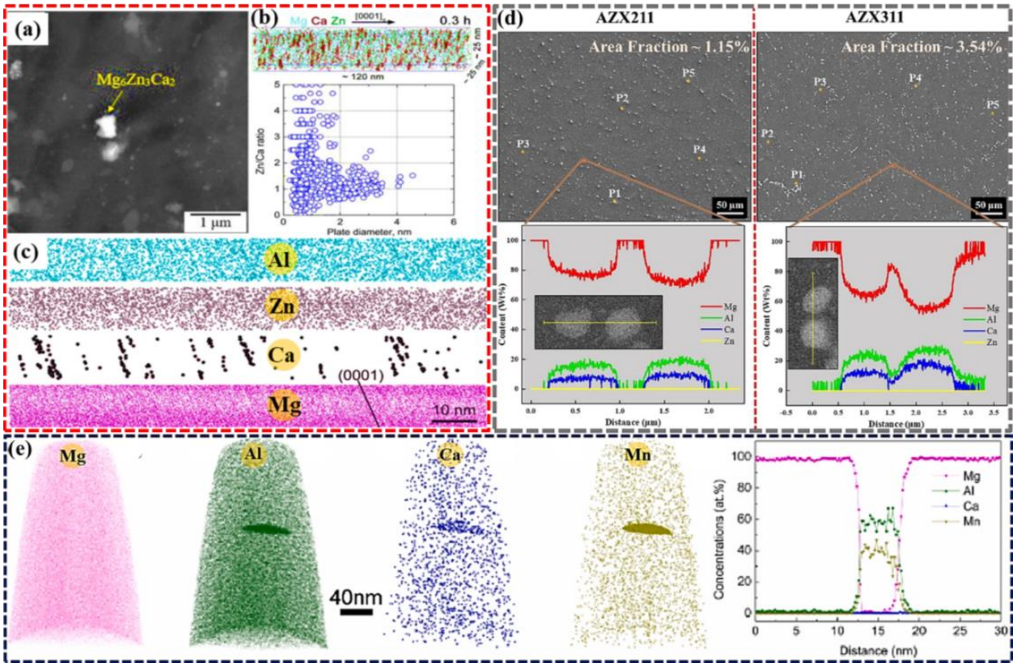



**Figure 3.** (**a**) TEM image showing precipitate formation and dispersion in Mg-Zn-Ca-Mn alloy; (**b**) 3D APT reconstruction image showing precipitation in Mg-0.3Ca; (**c**) 2D APT map showing distribution of Al, Zn, Ca, and Mg in ZAXME11100 alloy; (**d**) SEM images and EDS maps showing precipitate formation in AZX211 and AZX311 alloys; (**e**) 3D APT reconstruction image and line profile showing precipitate formation and their composition in Mg-3Al-1Ca-1Mn alloy (all figures reprinted from [49,65–69]).

## 3. Texture Modifications Caused by RE and Non-RE Alloying Additions

Mg alloys, with their HCP structure, exhibit distinct plasticity governed by limited crystallographic slip. At room temperature, only three basal slip systems with low CRSS are active, inherently restricting ductility due to insufficient independent slip systems [70]. Moreover, basal textures, often introduced during primary processing, orient grains to have a <c-axis> normal to the processing direction, and basal slips tend to have low Schmid factors in these cases, making ductility even lower. To further improve room-temperature ductility, the basal texture needs to be weakened or other non-basal slip systems need to be activated [71]. The alloying of Mg with RE elements enables the development of such an annealing texture with an off-basal pole spread deviating from the normal direction, driven by unique solute interactions and recrystallization mechanisms [72]. Among these, the mechanisms investigated to contribute to this unique texture evolution include particle-stimulated nucleation [73], deformation-induced twin nucleation [74], and shear band nucleation [75]. These processes are thought to favor the nucleation of recrystallized grains with either random or off-basal orientations. Since these mechanisms can also operate in Mg alloys without RE additions, the precise factors responsible for the distinctive texture in Mg-RE alloys are still under investigation.

Recent studies have pointed out the role of RE solutes in promoting oriented nucleation and growth during recrystallization [76]. Most importantly, the presence of RE-specific textures in dilute alloys evidences that the RE additions are mainly in the solution. For instance, Zhao et al. [77] demonstrated the effect of Y alloying on the texture modification of Mg-Y alloys during hot extrusion. The macrotexture evolution in Mg-Y alloys, shown in Figure 4a, reveals that the {0001} plane is concentrically spread around the extrusion direction at an angle of about 45° from it. The maximum intensity of the macrotexture decreases sharply from 3.89 to 2.61 with increasing Y content from 1 wt.% to 3 wt.%.

This progressive weakening of the texture suggests that Y addition promotes a more randomized grain orientation. This effect is further elucidated by the decrease in the c/a ratio of Mg alloys due to Y addition, which promotes non-basal slip during deformation. In this way, the basal planes of grains preferentially align with the extrusion direction. Grain orientations of this type alter the Schmid factor, which influences the selection of slip systems. Ansari et al. [78] also demonstrated the influence of an increase in the Y content of Mg-Y alloys on its texture and presented significant changes in the basal texture characteristics as shown in Figure 4b. In Mg-5Y, a strong basal texture is observed in the as-rolled state, wherein basal poles are concentrated along a particular orientation. This basal texture weakens after annealing, as reflected by the decrease in maximum texture intensity values. This weakening thus indicates a redistribution of crystallographic orientations during recrystallization. In contrast, the Mg-10Y alloy exhibited an inherently weaker basal texture, even in the as-rolled condition. Increased Y content further reduces the annealing texture strength; such a phenomenon indicates that increasing Y content effectively suppresses the strong basal orientation characteristic of Mg alloys. This is believed to be due to the higher solute concentration in Mg-10Y, which enhances grain boundary pinning and interferes with the homogeneity of basal texture development during recrystallization. Coupled with the increased Y content, an effective reduction in the intensity of texture is significant for improving formability in Mg-Y alloys. The addition of a high level of Y, such as in Mg-10Y, mitigates strong basal textures that limit ductility, thus enabling more isotropic deformation behavior [78].

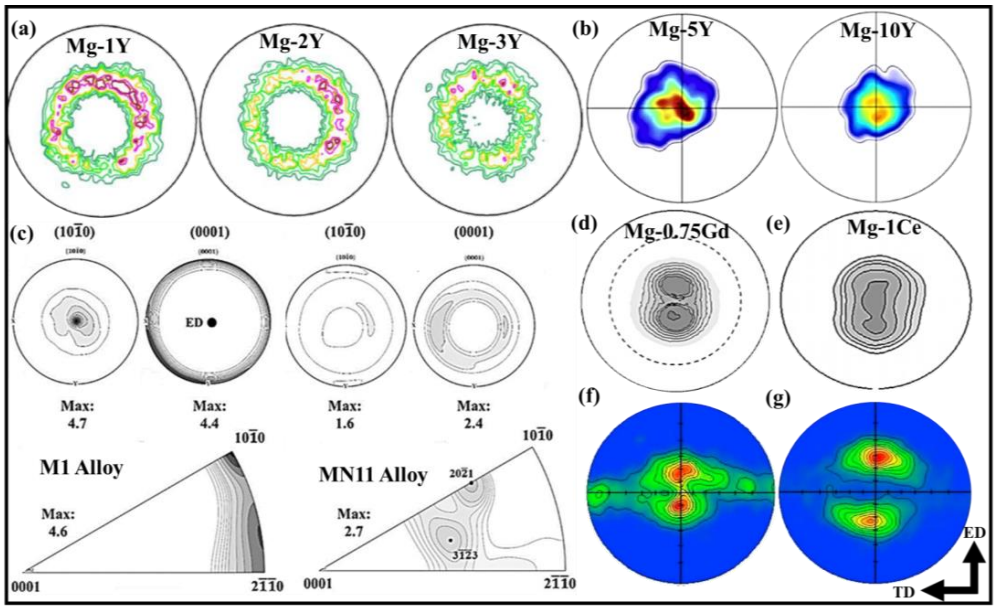



**Figure 4.** Texture variation with RE elements alloying (**a**) as-extruded Mg-1Y alloy, Mg-2Y alloy, and Mg-3Y alloy; (**b**) Mg-5Y alloy, and Mg-10Y alloy. (**c**) Recalculated (10-10) and (0001) pole figures and inverse pole figures of M1 and MN11 alloys; (**d**) pole figure for Mg-0.75Gd alloy; (**e**) pole figure for Mg-1Ce alloy, (**f**) Mg-0.5RE, and (**g**) Mg–2Zn–0.5RE (all figures are reprinted from [76–81]).

The addition of RE elements is very important for texture evolution in the Mg-Mn alloy due to the strong basal texture being profoundly weakened. Nd is also one of the most potential candidates for improvement in texture evolution, as it strongly influences recrystallization and activates slip systems [79]. It tends to weaken the basal texture by inducing lattice distortion and the solute drag effect that promotes the activity of non-basal slips. For example, Woo et al. studied the XRD-measured pole figures and inverse pole figures for the Mg-Mn (M1) and Mg-1Mn-1Nd (MN11) alloys, respectively (Figure 4c). According to their findings, it was revealed that the strong basal-type texture of most grains

with their basal planes parallel to ED was identified in the M1 alloy. The inverse pole figure further showed strong intensity along the arc spanning the <10-10> and <2-1-10> poles, which is a typical characteristic of conventionally extruded Mg alloys. The addition of Mn is in support of this kind of texture formation, enhancing the alignment of basal planes with ED. However, the MN11 alloy had a distinct texture characterized by basal poles tilted away from ED. The principal texture components of the MN11 alloy were <20-21> and <3-1-23>, and the texture intensity was far weaker than that of M1, amounting to 2.7 m.r.d. compared to 4.6 m.r.d. This was attributed to the addition of Nd, which acts to weaken the texture through promoting non-basal slip and dynamic recrystallization. It is also stated that the addition of 0.75 wt.% Gd to Mg weakened the strong basal texture. The intensity has shifted away from the center of the stereographic projection (Figure 4d). This suggests the redistribution of grain orientations that improve ductility by way of reducing anisotropic behavior. Similarly, the addition of Ce in the Mg-1Ce alloy also weakened the basal texture, as seen in Figure 4e, though the degree of modification differs compared with Gd. The excess of Ce lowers the CRSS required for the motion of dislocations on the slip systems <c + a>. It forms Mg-Ce phases, which precipitate and distort the more uniform structure and effectively pin different grain orientations.

It is also established that the addition of Zn in Mg-RE alloys can further suppress basal textures, thus promoting off-basal characteristics. It reflects a complex interaction mainly between the involved solutes with quite different atomic radii. Mg-Zn-RE (ZE) alloys develop a very distinctive texture after recrystallization upon rolling, characterized by the basal poles showing a marked split toward the TD of the sheet. The TD-spread texture has been reported in a few Mg-Zn-RE alloys with Ce, Gd, and Nd as the RE additions. The material usually has a basal pole spread toward the TD in the as-rolled condition and may retain some split toward the RD. However, this pronounced TD-oriented spread and split develop more clearly during recrystallization. These alloys have been given considerable attention owing to the improved formability conferred by their textures, which are superior to that of conventional Mg alloys and binary Mg-RE sheets. The texture of the Mg-0.5RE alloy is shown in Figure 4f, and the basal poles of most grains display a clear rotation from ND toward ED. This gives rise to a typical double-peak texture in the (0001) pole figure. However, Figure 4g shows the texture of the Mg-2Zn-0.5RE alloy, whose basal poles are distributed even more widely and exhibit a significant spread not only to ED but also to TD. The addition of Zn to the Mg-0.5RE alloy contributes to a further weakening of the texture intensity and enhances the dispersion of basal poles, emphasizing the synergistic effect of Zn and RE elements in achieving more isotropic texture characteristics [81].

Recent investigations have demonstrated that alloys containing Ca as an alloying addition to replace the RE elements also exhibit equivalent texture-modifying capabilities. Of these, the Mg-Ca-based alloys have received considerable interest because dilute additions of Ca have been shown to significantly weaken the basal texture and promote the activation of non-basal slip systems. According to Chaudry et al. [82], pure Mg generally develops a very strong c-axis texture with the majority of its grains strongly aligned along the ND and a small remaining tension twin component (Figure 5a). Such texture attained a maximum intensity of 23.81 m.r.d in their observation. In contrast, this basal texture of the Mg-Ca alloy significantly weakened and its peaks diffused along the RD and TD. It means that the basal pole intensities had come down drastically to 11.29 m.r.d in Mg-0.3Ca and 5.38 m.r.d in Mg-0.5Ca, further confirming the capability of Ca addition for the texture weakening. The mechanism behind such texture modification is reportedly due to the intermetallic Mg-Ca particles that induce PSN. These particles play a very important role in providing a grain boundary pinning effect that reduces the mobility of grain boundaries and hence hinders grain growth in the basal orientation. Furthermore, it was reported [64]

that the textural evolution of AZ61 alloys was highly influenced by the addition of CaO. The normal AZ61 alloy exhibits a very strong basal texture, and its maximum intensity was determined as 17.4 m.r.d of basal poles aligned along the ND. In the work, striking changes in texture were achieved with the addition of CaO. In the AZ61-0.5CaO alloy, a splitting of the basal poles towards the rolling direction takes place, together with a decrease in the basal pole intensity to 13.7 m.r.d. Further CaO addition, in the AZ61-1CaO alloy, leads to a further spreading of the basal poles perpendicular to the ND, indicating the weakening of the strong basal texture into non-basal texture components. This evolution, characterized by the development of texture components near the transverse direction, is influenced by second-phase particles that restrict preferential crystal alignment. While the AZ61-1CaO alloy has the highest texture intensity of 21.17 m.r.d, the overall distribution favors non-basal slip activity (Figure 5b).

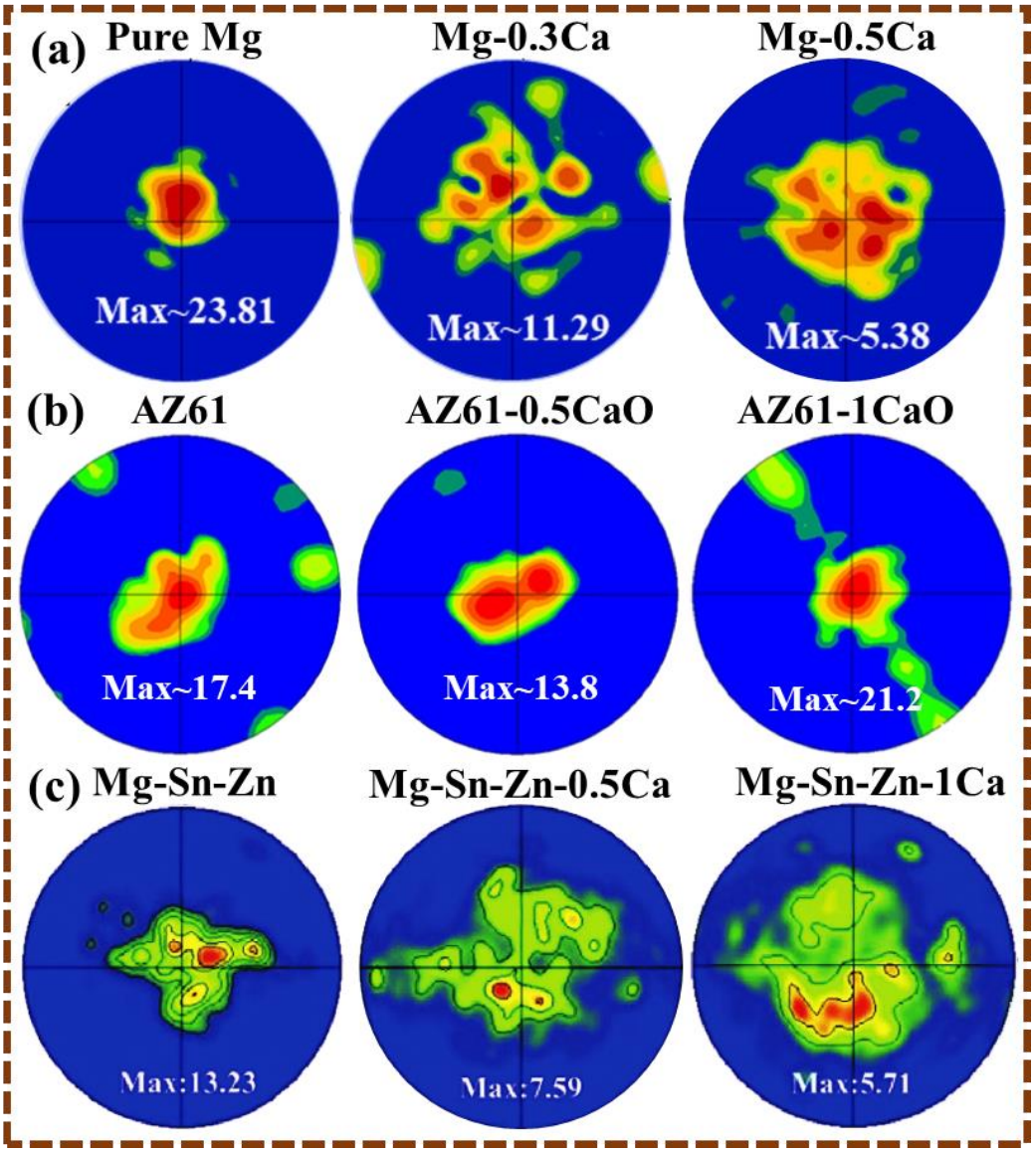



**Figure 5.** Pole figures showing texture variation with non-RE elements alloying (**a**) pure Mg, Mg-0.3Ca alloy, and Mg-0.5Ca alloy; (**b**) AZ61 alloy, AZ61-0.5CaO alloy, and AZ61-1CaO alloy; (**c**) Mg-Sn-Zn alloy, Mg-Szn-Zn-0.5Ca alloy, and Mg-Sn-Zn-1Ca alloy (all figures are reprinted from [64,82,83]).

The Mg-Sn-based alloys have been considered a promising pathway in the development of high-strength magnesium alloys free of rare-earth elements. In such systems, the limited solubility of Sb in the magnesium matrix leads to the precipitation of $Mg_3Sb_2$.

With an increase in the Sb content, the density of such precipitates increases; this favors non-spontaneous nucleation and grain growth restriction, thus refining the microstructure and improving the strength of the alloy. However, at higher concentrations of Sb, the phases of $Mg_3Sb_2$ tend to become coarse and segregated, thus affecting mechanical performance. The addition of Ca is particularly effective because it enhances texture modification by DRX and grain orientation adjustment. Chai et al. [83] reported that the addition of Ca from 0.5 wt.% to 1.0 wt.% in hot-extruded Mg-1.0Sn-0.5Zn alloys significantly weakens the strong basal texture, progressively transforming it into an ED-split texture. At 0.5 wt.% Ca, the basal texture starts to weaken due to the initiation of DRX and grain refinement. As the Ca content increases to 1.0 wt.%, the texture further weakens, transitioning into a split-type orientation (Figure 5c). With more of an increase, 2.0 wt.% Ca, the basal texture is effectively replaced by a weakened ED-split texture, with minimal anisotropy. This transformation is driven by refined grains, promoted by increased dynamic recrystallization, and the formation of secondary phases such as Ca-Mg-Sn and $Mg_2Ca$, which enhance non-basal activity, resulting in reduced tension–compression asymmetry and improved mechanical performance.

## 4. Corrosion Behavior of RE- and Non-RE-Based Mg Alloy

The standard potential of Mg~−2.37 V cannot prevent its degradation by the formation of an effective protective layer on it. The oxide layer formed on the Mg surface is porous and may not prevent Mg from further corrosion like steel, aluminum, or titanium [84]. Therefore, corrosion may occur in different forms, including uniform corrosion, galvanic corrosion, pitting, stress corrosion, and intergranular corrosion. The anodic and cathodic reactions responsible for the corrosion of Mg are given by Equations (1) and (2), respectively.

$$Mg + 2OH^- \rightarrow Mg(OH)_2 + 2e^- \quad (1)$$

$$2H_2O + 2e^- \rightarrow H_2 + 2OH^- \quad (2)$$

To improve the corrosion resistance of magnesium, alloying elements are incorporated to develop Mg alloys, or various coatings are applied to provide enhanced protection against corrosion [85]. However, alloying with other elements can create a potential difference between Mg and the alloying element, which may promote galvanic corrosion. Moreover, most of the precipitates or secondary phases formed through the alloying of Mg more cathodic compared to other Mg, which can lead to the formation of micro-galvanic cells, thereby degrading the overall corrosion resistance [86]. Therefore, selecting appropriate alloying elements and their optimal amounts is essential [87]. This discussion will summarize the corrosion resistance of Re and non-Re Mg alloys along with the underlying mechanisms. Alloying additions such as Al or Zn enhance corrosion resistance by promoting the formation of a protective surface layer or by acting as sacrificial elements, thereby shielding the magnesium alloy from further degradation [88,89]. Al can form the $Mg_{17}Al_{12}$ intermetallic phase and an al-rich protective layer on the Mg alloy to improve the corrosion resistance [90]. Mn can form complex compounds with other impurities like Fe in Mg and can help to improve the corrosion resistance [91]. Small additions of Ca can also improve the corrosion resistance of Mg by forming a protective $CaCO_3$ layer [92]. Similarly, lithium can also form a layer of $Li_2CO_3$, which can prevent Mg alloys from further corrosion [93].

RE elements have demonstrated significant potential as alloying additions to improve the corrosion resistance of Mg alloys either by reducing the galvanic cells [94], by formation or protective layers [95], or by improving the texture. For instance, the alloying of Mg with Nd enhances the (0001) basal texture, which helps to improve the corrosion resistance of Mg-Nd alloys [96]. Similarly, other RE elements, such as Gd, Y, and Er, have been reported

to enhance the corrosion resistance of Mg alloys by reducing the number of active galvanic cells and promoting the formation of protective surface films [97,98]. However, as discussed earlier, the formation of the secondary phase may accelerate the corrosion rate as reported by Shi et al. [96] and Birbilis et al. [99] for RE-based Mg alloys with Ce, La Gd, Nd, and Y additions.

To summarize, various Mg alloys with RE and non-RE elements, along with their corrosion rates in different media, are listed in Table 1.

**Table 1.** RE and non-RE Mg alloys and their corrosion rates in different media.

| Mg Alloy | Testing Media | Corrosion Rate (mm/year) |
|---|---|---|
| Mg-4Sn [100] | HBSS | 2.41 |
| Mg-4Sn-1Ce [100] | HBSS | 2.00 |
| Mg-4Sn-2Ce [100] | HBSS | 3.76 |
| Mg-4Sn-4Ce [100] | HBSS | 5.28 |
| MgCa4Zn1Gd1 [101] | Ringer's solution | 1.86 |
| MgCa4Zn1Gd2 [101] | Ringer's solution | 0.62 |
| MgCa4Zn1Gd3 [101] | Ringer's solution | 1.48 |
| Mg6Zn3Ag [102] | SBF | 22.01 |
| Mg7Zn1Ag [102] | SBF | 28.83 |
| Mg1Ca [102] | SBF | 31.24 |
| Mg-0.6Al-0.5Mn-0.2Ca [103] | 3.5 wt.% NaCl solution | 1.0 |
| Mg-0.6Al-0.5Mn-0.2Ca-0.3Ce [103] | 3.5 wt.% NaCl solution | 0.1 |
| Mg-1.88Al-1.88Ca [104] | 0.01M NaCl | 0.47 |
| Mg-3Al-2Ca-0.5Mn [104] | 0.01M NaCl | 0.23 |
| Mg-3Ca-0.3Mn-0.01Zn [105] | $Na_2SO_4$ solution | 16.03 |
| Mg-3.6Al-2.5Ca-0.5Mn0.01Zn [105] | $Na_2SO_4$ solution | 3.33 |
| Mg-0.5Mn-0.6Ca [106] | 3.5 wt.% NaCl solution | 0.64 |
| Mg-2Al-0.5Mn-0.7Ca [106] | 3.5 wt.% NaCl solution | 1.53 |
| Mg-9Sn-0.5Mn-0.7Ca [106] | 3.5 wt.% NaCl solution | 2.02 |
| Mg-4Zn-0.5Mn-0.7Ca [106] | 3.5 wt.% NaCl solution | 0.46 |
| Mg-4Zn-0.7Zr-0.4Ce-0.1La-0.1Nd [107] | HBSS | 13.7 |
| Mg-3Zn-1.3Zr-1.2Ce-0.5La-0.1Nd [107] | HBSS | 5.0 |

## 5. Impact of RE and Non-RE Alloying on Strength and Ductility of Mg Alloys

To achieve better synergy in strength and ductility through RE addition and the formation of stable precipitates, RE-containing Mg alloys have been continuously explored for their enhanced performance [108]. Among RE elements, lanthanum (La), cerium (Ce), neodymium (Nd), Samarium (Sm), gadolinium (Gd), Dysprosium (Dy), and yttrium (Y) are some of the RE elements that researchers commonly add to Mg alloys. The effect of each RE element in detail is beyond the scope of this short review. Therefore, we will provide a concise overview of how these elements form precipitates and how these precipitates contribute to the strengthening of Mg alloys.

The limited solubility of individual RE elements in Mg has led to the practice of adding multiple RE elements to form RE-Mg alloys. The addition of RE elements to Mg alloys leads to the formation of a super-saturated solid solution, which subsequently evolves into GP zones, followed by transitions to β″, β′ (bcc), and finally β (fcc) phases [109]. These precipitates and phases contribute to hardening effects. For instance, the addition of 8 wt.% Gd and 3 wt.% Nd to Mg results in a UTS of 271 MPa [110], while 7 wt.% Gd and 5 wt.% Y yield a UTS of 258 MPa [111]. Incorporating Gd, Nd, and Y together in an alloy (Mg-8Gd-2Nd-1Y) achieves an even higher UTS of 293 MPa [112]. A UTS of 355 MPa has been reported for the Mg-8Gd-1Dy-0.4Zr alloy, attributed to the presence of finely dispersed $Mg_{15}RE_2$ and $Mg_5RE$ precipitates [113]. These precipitates enhance the

mechanical strength of RE-Mg alloys by hindering dislocation slip on the basal planes. The overall mechanical properties can be improved through the combined presence of prismatic β- and basal γ-precipitates. These precipitates can align at right angles to form a compact structure, effectively blocking dislocation motion and thereby enhancing the strength of the alloy [114].

These precipitates typically exhibit a melting temperature higher than that of Mg, providing superior thermal stability. This characteristic enhances their ability to contribute effectively to the hardening of Mg alloys, even at elevated temperatures. The improved thermal stability of these phases ensures that they remain effective in impeding dislocation motion under high-temperature conditions, thereby maintaining the mechanical strength of the alloy. Table 2 provides an overview of some of the most common phases in RE-Mg alloys along with their respective melting points. The morphology of these precipitates also plays a crucial role in determining the final mechanical behavior, as it directly influences how they strengthen the matrix. Various morphologies, such as globular and plate-like, have been reported in the literature, as shown by TEM images (Figure 6a) for the Mg-Y-RE-Zr alloy [115] and APT reconstruction images and line profiles (Figure 6b) for the Mg-2Nd-4Y-0.5Ca alloy [116].

**Table 2.** Precipitates/phases in Mg alloys and their melting points (M.P.) [117].

| RE-Mg Alloy | Precipitates/Phase | M.P. °C | RE-Mg Alloy | Precipitates/Phase | M.P. °C |
|---|---|---|---|---|---|
| Mg-Al | $Mg_{17}Al_{12}$ | 455 | Mg-Yb | $Mg_2Yb$ | 718 |
| Mg-La | $Mg_{12}La$ | 640 | Mg-Y | $Mg_{24}Y_5$ | 605 |
| Mg-Ce | $Mg_{12}Ce$ | 611 | Mg-Al-La | $Al_{11}La_3$ | 1240 |
| Mg-Nd | $Mg_{41}Nd_5$ | 560 | Mg-Al-Ce | $Al_{11}$ $Ce_3$ | 1235 |
| Mg-Gd | $Mg_5Gd$ | 642 | Mg-Al-Ce | $Al_2$ -Ce | 1480 |
| Mg-Dy | $Mg_{24}Dy_5$ | 610 | Mg-Al-Nd | $Al_{11}$ $Nd_3$ | 1235 |
| Mg-Ho | $Mg_{24}Ho_5$ | 610 | Mg-Al-Nd | $Al_2Nd$ | 1460 |
| Mg-Er | $Mg_{24}Er_5$ | 610 | Mg-Al-Y | $Al_2Y$ | 1485 |

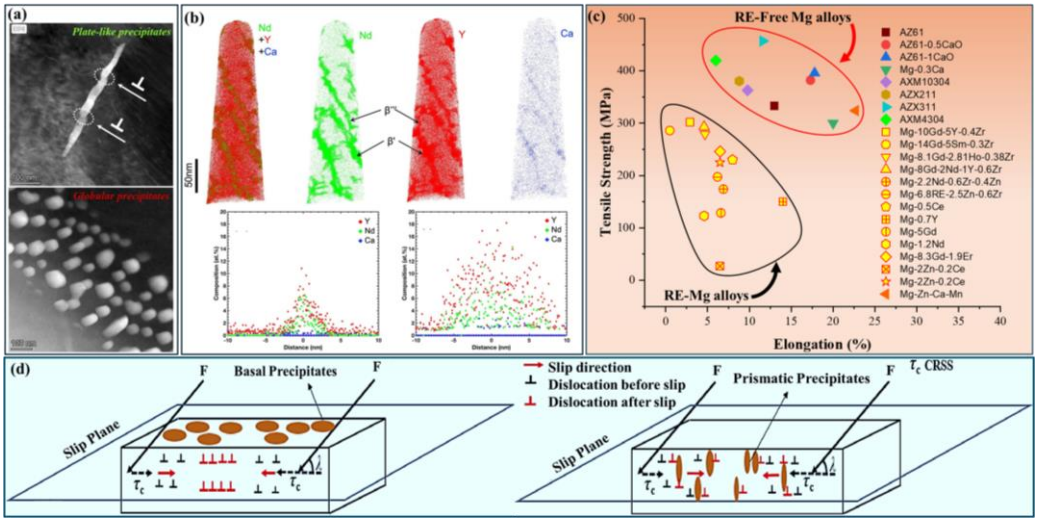



**Figure 6.** Morphologies of RE-rich precipitates in (**a**) TEM images of the Mg-Y-RE-Zr alloy (figure is reprinted from [115]), (**b**) APT reconstruction images and line profiles for the Mg-2Nd-4Y-0.5Ca alloy (reprinted from [116]) (**c**) A scatter plot comparing the tensile strength and elongation of various Mg alloys containing RE and non-RE elements [16,64,82,118–130]. (**d**) A schematic illustration demonstrating how the orientation of precipitate plates influences dislocation glide on the basal plane within the Mg matrix [131].

Nie [132] proposed an updated version of the Orowan equation to predict the strengthening effects of basal and prismatic precipitates, as represented by Equations (3) and (4), respectively.

$$\Delta\tau = \frac{Gb}{2\pi\sqrt{1 - v\left(\frac{0.953}{\sqrt{f}} - 1\right)D}} ln\frac{D}{b} \quad (3)$$

$$\Delta\tau = \frac{Gb}{2\pi\sqrt{1 - v\left(0.825\sqrt{\frac{DT}{f}} - 0.393D - 0.886T\right)}} ln\frac{0.886\sqrt{DT}}{b} \quad (4)$$

Here, $D$ is the diameter, $T$ is the thickness, and $f$ is the volume fraction of precipitates.

According to Nie [132], in addition to the shear modulus ($G$) and Burgers vector ($b$), the diameter, thickness, and volume fraction of the developed precipitates also play a crucial role in determining the overall strengthening effect.

It is well known that strengthening effects from prismatic precipitates are more pronounced in general than those from basal precipitates. A schematic diagram is included to show more clearly the different types of hardening effects for basal slip from the two types of precipitates [131]. The influence of basal and prismatic precipitates upon dislocation glide along the basal plane of the Mg matrix is depicted in Figure 6d. The slip plane is designated as basal of the Mg matrix, with dislocation motion direction illustrated in red arrows. The black dislocations show their position before slipping while the red dislocations indicate after slipping positions. Both basal and prismatic precipitates are inserted into the Mg matrix accordingly. The conceptual scheme merely suggests that basal precipitates exert a little blocking effect on dislocation motion, which results in a very small critical resolved shear stress ($\Delta\tau$). Because of this, basal slip is rendered more easily, and so magnesium alloys with basal precipitates would tend to be of lesser strength. On the contrary, prismatic precipitates cause more blocking to dislocation motion, leading to a higher value of $\Delta\tau$. Accordingly, basal slip is restricted more, and thus magnesium alloys having prismatic precipitates are generally high in strength.

Processing techniques such as extrusion, rolling, and heat treatment play critical roles in determining the size, density, and distribution of these strengthening phases, thereby ensuring a favorable combination of strength and ductility in Mg-RE alloys. By increasing <c + a> slip activity, RE elements are efficient at improving the ductility of Mg alloys. For large-scale industrial uses of Mg-RE alloys, however, their high cost, manufacturing complexity, and lack of recyclability pose critical obstacles. Several alloying elements have been found to be viable options that provide similar processes for improving the mechanical performance of Mg alloys, hence increasing their suitability for wider applications. For instance, when a small amount of Mn (0–0.3 wt.%) is added to an Mg-Al-Ca alloy, both the yield strength (YS) and elongation (EL) are improved. The YS increases from 366 MPa (at 0% Mn) to approximately 400 MPa with just 0.3 wt.% Mn addition, while the elongation enhances from about 2.8% to around 4% [133]. Similarly, the addition of Ca in the range of 2–6 wt.% to an Mg-6Al alloy significantly enhances the YS. The YS increases from 248 MPa at 2.6 wt.% Ca to 289 MPa at 3.68 wt.% Ca and reaches 404 MPa with 5.78 wt.% Ca. This improvement is attributed to the formation of various nanosized precipitates like $Al_2Ca$ or $(Mg, Al)_2Ca$ [134]. These strength values surpass those achieved with the addition of RE elements in alloys such as Mg-17Gd-0.5Zr (YS = 278 MPa) [114], Mg-10Gd-5Y-0.4Zr (YS = 289 MPa) [135], Mg-11Gd-2Nd-0.5Zr (YS = 231 MPa) [12], Mg-14Gd-5Sm-0.3Zr (YS = 262 MPa) [136], Mg-8Gd-1Dy-0.4Zr (YS = 261 MPa) [113], Mg-8.1Gd-2.81Ho-0.38Zr (YS = 175 MPa) [137], Mg-8Gd-2Nd-1Y-0.6Zr (YS = 221 MPa) [112], and Mg-2Gd-2Y-2Nd-2Sm-1Ag-1Zn-0.5Zr (YS = 228 MPa) [138]. A more detailed comparison of strengths vs.

elongation to failure of RE and non-RE Mg alloys is also illustrated graphically, as shown in Figure 6c.

As the need for high-strength and -ductility Mg alloys for applications in the automotive, aerospace, and biomedical industries grows, both RE and non-RE alloying strategies cover a diverse landscape to optimize strength, ductility, and thermal stability. Although RE elements including Gd, Nd, and Y allow higher strengthening due to the stable precipitates and unique textures that they produce, they also represent a remaining challenge for cost and scalability. While non-RE elements such as Al, Ca, Zn, and Mn can be more economic, their influence on texture development and phase stability in a range of conditions has yet to be investigated. Moreover, optimizing novel sustainable and energy-efficient processing technologies such as advanced thermomechanical treatments and additive manufacturing is key for scaling up the production potential and industrial applicability of Mg alloys.

## 6. Conclusions

This study critically evaluates the influence of RE and non-RE alloying elements on the microstructural evolution, thermal stability, and mechanical properties of Mg alloys. The key findings are summarized as follows:

1. The addition of RE and non-RE alloying elements in Mg alloys significantly improves the grain refinement and mechanical properties, by solute segregation, heterogeneous nucleation, and dynamic recrystallization. RE elements with high grain refinement potential include Nd, Gd, and Zr due to their ability for constitutional super-cooling and to form intermetallic phases while non-RE elements (e.g., Al, Ca) are cheaper alternatives with comparable refinement efficacity. These alloying strategies can yield tailored microstructures and enhanced performance, all of which come with scalability constraints and composition optimization challenges.
2. By alloying Mg with the addition of RE and non-RE elements, the texture evolution is considerably modified with basal texture intensities reduced, and isotropic deformation mechanisms promoted. A translation of the basal texture is obtained when the RE-type elements (e.g., Y, Nd, Ce) dissolve, subsequently weakening the basal textures, while the non-RE elements (e.g., Ca, Zn) have been found to result in similar effects, which could ultimately activate non-basal slip systems and improve ductility and mechanical performance.
3. RE-alloyed Mg demonstrates superior strength and thermal stability, suitable for aerospace, biomedical, and electronics industries, but is very expensive. Non-RE alloys, like Ca and Mn, on the other hand, are cost-effective with good mechanical properties and hence suitable for automotive and structural applications that require economy and scalability.
4. The corrosion resistance of Mg is improved by alloying with Al, Zn, and Mn, with the subsequent development of protective oxide layers. For example, $Mg_{17}Al_{12}$ may form, along with a sacrificial anodic reaction. In general, RE elements such as Nd, Gd, Y, and Er improve corrosion resistance by the textural modification of the alloy to reduce the establishment of active galvanic cells, promoting the formation of stable protective films. However, cathodic secondary phases like intermetallic ones may form and contribute to localized corrosion through micro-galvanic coupling. The corrosion behavior thus depends not only on the choice and concentration of alloying elements but also on the interaction between the matrix and secondary phases, which may improve or degrade the overall corrosion resistance in various environments.

**Author Contributions:** Conceptualization, H.M.R.T. and M.I.; Methodology, H.M.R.T., M.I. and H.-H.K.; Formal analysis, H.M.R.T. and U.M.C.; Investigation, M.I. and H.-H.K.; Resources, M.I. and U.M.C.; Data curation, H.M.R.T. and M.I.; Writing—original draft, H.M.R.T., M.I. and H.-H.K.; Writing—review and editing, T.-S.J. and U.M.C.; Supervision, T.-S.J.; Project administration, T.-S.J.; Funding acquisition, T.-S.J. All authors have read and agreed to the published version of the manuscript.

**Funding:** This work was supported by a National Research Foundation of Korea (NRF) grant funded by the Korean government (MSIT) (No. 2020R1C1C1004434).

**Data Availability Statement:** The original contributions presented in the study are included in the article, further inquiries can be directed to the corresponding author.

**Conflicts of Interest:** The authors declare no conflicts of interest.

## Abbreviations

The following abbreviations are used in this manuscript:

| | |
|---|---|
| RE | Rare Earth |
| M.P. | Melting Point |
| YS | Yield Strength |
| EL | Elongation |
| GP | Guinier–Preston |
| GRF | Grain Restriction Factor |
| SEM | Scanning Electron Microscopy |
| OM | Optical Microscopy |
| EDS | Energy Dispersive Spectroscopy |
| TEM | Transmission Electron Microscopy |
| APT | Atom Probe Tomography |
| EBSD | Electron Backscattered Diffraction |
| RD | Rolling Direction |
| TD | Transverse Direction |
| ND | Normal Direction |
| ED | Extrusion Direction |
| HCP | Hexagonal Close-packed |
| CRSS | Critical Resolved Shear Stress |

## References

1. Zhang, W.; Xu, J. Advanced lightweight materials for Automobiles: A review. *Mater. Des.* **2022**, *221*, 110994. [CrossRef]
2. Li, A.; Qiao, Y.; Fu, S.; Gu, Y. An analysis of new materials and their effects on improving fuel efficiency. *J. Phys. Conf. Ser.* **2022**, *2194*, 012001. [CrossRef]
3. Kulekci, M.K. Magnesium and its alloys applications in automotive industry. *Int. J. Adv. Manuf. Technol.* **2008**, *39*, 851–865. [CrossRef]
4. Mordike, B.; Ebert, T. Magnesium: Properties—Applications—Potential. *Mater. Sci. Eng. A* **2001**, *302*, 37–45. [CrossRef]
5. Chaudry, U.M.; Jun, T.-S.; Tariq, H.M.R.; Minhas, B.Z.; Rehman, M.A.U. Corrosion Behavior of Mg Alloys in Simulated Body Fluids. In *Magnesium Alloys for Biomedical Applications*; CRC Press: Boca Raton, FL, USA, 2024; pp. 177–188.
6. Khan, M.A.; Afifi, M.A.; Hafeez, M.A.; Chaudry, U.M.; Brechtl, J.; Zulfiqar, M.; Tariq, H.M.R.; Hussain, M.A.; Kamran, M.; ishtiaq, M. Evolution of microstructure, texture, and mechanical performance of Mg-13Gd-2Er-0.3 Zr alloy by double extrusion at different temperatures. *Arch. Civ. Mech. Eng.* **2024**, *25*, 26. [CrossRef]
7. Hussain, F.; Manzoor, M.U.; Kamran, M.; Ahmad, T.; Riaz, F.; Mukhtar, S.; Rehan Tariq, H.M.; Ishtiaq, M. Optimizing Biocompatibility of Mg-AZ31B Alloy through Varied Surface Roughness and Anodization Time. *Iran. J. Mater. Sci. Eng.* **2024**, *21*. [CrossRef]
8. Chaudry, U.M.; Rehan Tariq, H.M.; Hamad, K.; Khan, M.K.; Jun, T.-S. Twinning-induced texture weakening in Mg alloy and its consequent influence on ductility and formability. *Mater. Sci. Technol.* **2024**, *41*, 02670836241251942. [CrossRef]

9. Xu, W.; Yu, J.; Jia, L.; Gao, C.; Miao, Z.; Wu, G.; Li, G.; Zhang, Z. Grain refinement impact on the mechanical properties and wear behavior of Mg-9Gd-3Y-2Zn-0.5Zr alloy after decreasing temperature reciprocating upsetting-extrusion. *J. Magnes. Alloys* **2022**, *10*, 3506–3519. [CrossRef]
10. Sun, M.; Yang, D.; Zhang, Y.; Mao, L.; Li, X.; Pang, S. Recent Advances in the Grain Refinement Effects of Zr on Mg Alloys: A Review. *Metals* **2022**, *12*, 1388. [CrossRef]
11. Yang, Z.; Li, J.P.; Guo, Y.C.; Liu, T.; Xia, F.; Zeng, Z.W.; Liang, M.X. Precipitation process and effect on mechanical properties of Mg–9Gd–3Y–0.6Zn–0.5Zr alloy. *Mater. Sci. Eng. A* **2007**, *454–455*, 274–280. [CrossRef]
12. Zheng, K.Y.; Dong, J.; Zeng, X.Q.; Ding, W.J. Precipitation and its effect on the mechanical properties of a cast Mg–Gd–Nd–Zr alloy. *Mater. Sci. Eng. A* **2008**, *489*, 44–54. [CrossRef]
13. Wang, J.-Y.; Saufan, A.; Lin, P.H.; Bor, H.Y.; Lee, S.; Kawamura, Y. Mechanical properties and strengthening behavior of Mg–Zn–MM alloy. *Mater. Chem. Phys.* **2014**, *148*, 28–31. [CrossRef]
14. Guo, F.; Yu, H.; Wu, C.; Xin, Y.; He, C.; Liu, Q. The mechanism for the different effects of texture on yield strength and hardness of Mg alloys. *Sci. Rep.* **2017**, *7*, 8647. [CrossRef] [PubMed]
15. Stráská, J.; Minárik, P.; Šašek, S.; Veselý, J.; Bohlen, J.; Král, R.; Kubásek, J. Texture Hardening Observed in Mg–Zn–Nd Alloy Processed by Equal-Channel Angular Pressing (ECAP). *Metals* **2020**, *10*, 35. [CrossRef]
16. Tekumalla, S.; Seetharaman, S.; Almajid, A.; Gupta, M. Mechanical Properties of Magnesium-Rare Earth Alloy Systems: A Review. *Metals* **2015**, *5*, 1–39. [CrossRef]
17. Wang, M.; Yu, H.L.; Chen, Y.; Huang, M.X. Machine learning assisted screening of non-rare-earth elements for Mg alloys with low stacking fault energy. *Comput. Mater. Sci.* **2021**, *196*, 110544. [CrossRef]
18. Tan, J.; Ramakrishna, S. Applications of Magnesium and Its Alloys: A Review. *Appl. Sci.* **2021**, *11*, 6861. [CrossRef]
19. Bai, J.; Yang, Y.; Wen, C.; Chen, J.; Zhou, G.; Jiang, B.; Peng, X.; Pan, F. Applications of magnesium alloys for aerospace: A review. *J. Magnes. Alloys* **2023**, *11*, 3609–3619. [CrossRef]
20. Jin, S.-C.; Cha, J.W.; Go, J.; Bae, J.H.; Park, S.H. Comparative study of extrudability, microstructure, and mechanical properties of AZ80 and BA53 alloys. *J. Magnes. Alloys* **2023**, *11*, 249–258. [CrossRef]
21. Go, J.; Jin, S.-C.; Kim, H.; Yu, H.; Park, S.H. Novel Mg–Bi–Al alloy with extraordinary extrudability and high strength. *J. Alloys Compd.* **2020**, *843*, 156026. [CrossRef]
22. Go, J.; Lee, J.U.; Yu, H.; Park, S.H. Influence of Bi addition on dynamic recrystallization and precipitation behaviors during hot extrusion of pure Mg. *J. Mater. Sci. Technol.* **2020**, *44*, 62–75. [CrossRef]
23. Park, S.H.; Kim, Y.J.; Kim, H.J.; Jin, S.-C.; Lee, J.U.; Komissarov, A.; Shin, K.S. Recent research progress on magnesium alloys in Korea: A review. *J. Magnes. Alloys* **2023**, *11*, 3545–3584. [CrossRef]
24. Jayasathyakawin, S.; Ravichandran, M.; Baskar, N.; Anand Chairman, C.; Balasundaram, R. Mechanical properties and applications of Magnesium alloy—Review. *Mater. Today Proc.* **2020**, *27*, 909–913. [CrossRef]
25. Wu, G.; Tong, X.; Wang, C.; Jiang, R.; Ding, W. Recent advances on grain refinement of magnesium rare-earth alloys during the whole casting processes: A review. *J. Magnes. Alloys* **2023**, *11*, 3463–3483. [CrossRef]
26. Atrens, A.; Shi, Z.; Mehreen, S.U.; Johnston, S.; Song, G.-L.; Chen, X.; Pan, F. Review of Mg alloy corrosion rates. *J. Magnes. Alloys* **2020**, *8*, 989–998. [CrossRef]
27. Zeng, R.-c.; Zhang, J.; Huang, W.-j.; Dietzel, W.; Kainer, K.U.; Blawert, C.; Ke, W. Review of studies on corrosion of magnesium alloys. *Trans. Nonferrous Met. Soc. China* **2006**, *16*, s763–s771. [CrossRef]
28. Hsu, Y.; Lu, Y.; Wang, S.; Zheng, Y.; Xia, D.; Liu, Y. Magnesium alloys in tumor treatment: Current research status, challenges and future prospects. *J. Magnes. Alloys* **2023**, *11*, 3399–3426. [CrossRef]
29. Zhang, T.; Wang, W.; Liu, J.; Wang, L.; Tang, Y.; Wang, K. A review on magnesium alloys for biomedical applications. *Front. Bioeng. Biotechnol.* **2022**, *10*, 953344. [CrossRef] [PubMed]
30. Gu, X.-N.; Zheng, Y.-F. A review on magnesium alloys as biodegradable materials. *Front. Mater. Sci. China* **2010**, *4*, 111–115. [CrossRef]
31. Czerwinski, F. Magnesium research in Canada: Highlights of the last two decades. *J. Magnes. Alloys* **2023**, *11*, 3484–3510. [CrossRef]
32. Li, Y.; Zhang, A.; Li, C.; Xie, H.; Jiang, B.; Dong, Z.; Jin, P.; Pan, F. Recent advances of high strength Mg-RE alloys: Alloy development, forming and application. *J. Mater. Res. Technol.* **2023**, *26*, 2919–2940. [CrossRef]
33. Zhang, J.; Liu, S.; Wu, R.; Hou, L.; Zhang, M. Recent developments in high-strength Mg-RE-based alloys: Focusing on Mg-Gd and Mg-Y systems. *J. Magnes. Alloys* **2018**, *6*, 277–291. [CrossRef]
34. Imandoust, A.; Barrett, C.D.; Al-Samman, T.; Inal, K.A.; El Kadiri, H. A review on the effect of rare-earth elements on texture evolution during processing of magnesium alloys. *J. Mater. Sci.* **2017**, *52*, 1–29. [CrossRef]
35. Wang, L.; Dong, Z.; Jiang, B.; Wang, C.; Qian, X.; Vitos, L.; Pan, F. Influence of non-rare earth elements on basal stacking fault energy of Mg binary alloys in solid solution. *Scr. Mater.* **2025**, *257*, 116479. [CrossRef]

36. Yuan, X.; Liu, M.; Wei, K.; Li, F.; Li, X.; Zeng, X. Defect, microstructure and mechanical properties of Mg–Gd binary alloy additively manufactured by selective laser melting. *Mater. Sci. Eng. A* **2022**, *850*, 143572. [CrossRef]
37. Wang, J.; Chang, Z.; Liu, B.; Li, Y.; Sun, Y.; Li, H. Effect of Y Alloying on Microstructure and Mechanical Properties of AZ61 Magnesium Alloy Sheets Applied as 3C Electronic Product Shells. *Crystals* **2022**, *12*, 1643. [CrossRef]
38. Qiu, D.; Zhang, M.X.; Taylor, J.A.; Kelly, P.M. A new approach to designing a grain refiner for Mg casting alloys and its use in Mg–Y-based alloys. *Acta Mater.* **2009**, *57*, 3052–3059. [CrossRef]
39. Natarajan, A.R.; Solomon, E.L.S.; Puchala, B.; Marquis, E.A.; Van der Ven, A. On the early stages of precipitation in dilute Mg–Nd alloys. *Acta Mater.* **2016**, *108*, 367–379. [CrossRef]
40. Gavras, S.; Easton, M.A.; Gibson, M.A.; Zhu, S.; Nie, J.-F. Microstructure and property evaluation of high-pressure die-cast Mg–La–rare earth (Nd, Y or Gd) alloys. *J. Alloys Compd.* **2014**, *597*, 21–29. [CrossRef]
41. Mishra, R.K.; Brahme, A.; Sabat, R.K.; Jin, L.; Inal, K. Twinning and texture randomization in Mg and Mg-Ce alloys. *Int. J. Plast.* **2019**, *117*, 157–172. [CrossRef]
42. Yu, H.; Xin, Y.; Wang, M.; Liu, Q. Hall-Petch relationship in Mg alloys: A review. *J. Mater. Sci. Technol.* **2018**, *34*, 248–256. [CrossRef]
43. Tong, X.; Wu, G.; Zhang, L.; Wang, Y.; Liu, W.; Ding, W. Microstructure and mechanical properties of repair welds of low-pressure sand-cast Mg–Y–RE–Zr alloy by tungsten inert gas welding. *J. Magnes. Alloys* **2022**, *10*, 180–194. [CrossRef]
44. Li, M.; Xie, D.; Li, J.; Xie, H.; Huang, Q.; Pan, H.; Qin, G. Realizing ultra-fine grains and ultra-high strength in conventionally extruded Mg-Ca-Al-Zn-Mn alloys: The multiple roles of nano-precipitations. *Mater. Charact.* **2021**, *175*, 111049. [CrossRef]
45. StJohn, D.H.; Qian, M.; Easton, M.A.; Cao, P.; Hildebrand, Z. Grain refinement of magnesium alloys. *Metall. Mater. Trans. A* **2005**, *36*, 1669–1679. [CrossRef]
46. Qian, X.; Dong, Z.; Jiang, B.; Zhang, A.; Wang, C.; Zheng, Z.; Pan, F. The improved mechanical properties of Mg–Zn-Nd alloy with Ca addition via grain refinement and nano precipitates. *Mater. Sci. Eng. A* **2023**, *887*, 145729. [CrossRef]
47. Ma, Q.; StJohn, D.H.; Frost, M.T. Characteristic zirconium-rich coring structures in Mg–Zr alloys. *Scr. Mater.* **2002**, *46*, 649–654. [CrossRef]
48. Cai, S.; Lei, T.; Li, N.; Feng, F. Effects of Zn on microstructure, mechanical properties and corrosion behavior of Mg–Zn alloys. *Mater. Sci. Eng. C* **2012**, *32*, 2570–2577. [CrossRef]
49. Niu, R.-L.; Yan, F.-J.; Wang, Y.-S.; Duan, D.-P.; Yang, X.-M. Effect of Zr content on damping property of Mg–Zr binary alloys. *Mater. Sci. Eng. A* **2018**, *718*, 418–426. [CrossRef]
50. Zhang, Y.; Yu, S.; Zhu, X.; Luo, Y. Study on as-cast microstructures and solidification process of Mg–Zn–Y Alloys. *J. Non-Cryst. Solids* **2008**, *354*, 1564–1568. [CrossRef]
51. Prasad, A.; Yuan, L.; Lee, P.D.; StJohn, D.H. The Interdependence model of grain nucleation: A numerical analysis of the Nucleation-Free Zone. *Acta Mater.* **2013**, *61*, 5914–5927. [CrossRef]
52. Qian, M.; Zheng, L.; Graham, D.; Frost, M.; StJohn, D. Settling of undissolved zirconium particles in pure magnesium melts. *J. Light Met.* **2001**, *1*, 157–165. [CrossRef]
53. Zhang, L.; Cao, Z.Y.; Liu, Y.B.; Su, G.H.; Cheng, L.R. Effect of Al content on the microstructures and mechanical properties of Mg–Al alloys. *Mater. Sci. Eng. A* **2009**, *508*, 129–133. [CrossRef]
54. Khan, M.U.F.; Mirza, F.; Gupta, R.K. High hardness and thermal stability of nanocrystalline Mg–Al alloys synthesized by the high-energy ball milling. *Materialia* **2018**, *4*, 406–416. [CrossRef]
55. Zhang, M.X.; Kelly, P.M. Edge-to-edge matching and its applications: Part II. Application to Mg–Al, Mg–Y and Mg–Mn alloys. *Acta Mater.* **2005**, *53*, 1085–1096. [CrossRef]
56. Liu, X.; Liu, F.; Liu, Z.; Xie, H.; Li, J. Crystal structure, phase content, and tensile properties of As-cast Mg–Gd–Y–Al alloys. *Mater. Today Commun.* **2020**, *25*, 101286. [CrossRef]
57. Su, N.; Wu, Q.; Ding, C.; Wu, Y.; Peng, L. Effect of Y and Gd solutes on grain refinement of the as-extruded Mg-Gd(-Y)-Zn-Mn alloys. *J. Alloys Compd.* **2023**, *968*, 171804. [CrossRef]
58. Cao, Y.; Wang, L.; Guo, E.; Zhao, S.; Fu, Y.; Fan, R.; Feng, Y. Grain refinement and exceptional creep resistance achieved in an as-cast Mg–Y alloy with Al addition. *Mater. Sci. Eng. A* **2024**, *901*, 146587. [CrossRef]
59. Fan, Y.; Zhu, G.; Park, J.-S.; Zhang, X.; Song, Z.; Wang, H.; Zeng, X.; Wang, L. The role of Ca on the microstructure and tensile properties of Mg-Al-Zn-Ca alloys. *Materialia* **2023**, *29*, 101787. [CrossRef]
60. Wang, Y.; Guan, S.; Zeng, X.; Ding, W. Effects of RE on the microstructure and mechanical properties of Mg–8Zn–4Al magnesium alloy. *Mater. Sci. Eng. A* **2006**, *416*, 109–118. [CrossRef]
61. Sasaki, T.T.; Yamamoto, K.; Honma, T.; Kamado, S.; Hono, K. A high-strength Mg–Sn–Zn–Al alloy extruded at low temperature. *Scr. Mater.* **2008**, *59*, 1111–1114. [CrossRef]
62. Mendis, C.L.; Oh-ishi, K.; Hono, K. Enhanced age hardening in a Mg–2.4at.% Zn alloy by trace additions of Ag and Ca. *Scr. Mater.* **2007**, *57*, 485–488. [CrossRef]

63. Li, Y.; Liang, Z.; Yang, L.; Zhao, W.; Wang, Y.; Yu, H.; Qin, C.; Wang, Z. Surface morphologies and mechanical properties of Mg-Zn-Ca amorphous alloys under chemistry-mechanics interactive environments. *Metals* **2019**, *9*, 327. [CrossRef]
64. Chaudry, U.M.; Tariq, H.M.R.; Ansari, N.; Lee, S.Y.; Jun, T.-S. Room and cryogenic deformation behavior of AZ61 and AZ61-xCaO (x = 0.5, 1 wt.%) alloy. *J. Magnes. Alloys* **2024**, *12*, 1996–2009. [CrossRef]
65. Kavyani, M.; Ebrahimi, G.R.; Ezatpour, H.R.; Jahazi, M. Microstructure refinement, mechanical and biocorrosion properties of Mg–Zn–Ca–Mn alloy improved by a new severe plastic deformation process. *J. Magnes. Alloys* **2022**, *10*, 1640–1662. [CrossRef]
66. Nakata, T.; Xu, C.; Ajima, R.; Shimizu, K.; Hanaki, S.; Sasaki, T.T.; Ma, L.; Hono, K.; Kamado, S. Strong and ductile age-hardening Mg-Al-Ca-Mn alloy that can be extruded as fast as aluminum alloys. *Acta Mater.* **2017**, *130*, 261–270. [CrossRef]
67. Jin, C.; Liu, Z.; Yu, W.; Qin, C.; Yu, H.; Wang, Z. Biodegradable Mg–Zn–Ca-Based Metallic Glasses. *Materials* **2022**, *15*, 2172. [CrossRef]
68. Miao, J.; Xue, F.; Liu, T.; Avey, T.; Marquis, E.A.; Luo, A.A. Achieving high strength-ductility synergy via Guinier-Preston zone formation in a new Mg–Zn–Al–Ca–Mn–Ce sheet alloy. *Mater. Sci. Eng. A* **2024**, *901*, 146586. [CrossRef]
69. Tariq, H.M.R.; Chaudry, U.M.; Ishtiaq, M.; Kim, M.; Ali, M.; Jun, T.-S. Effect of Al addition on the room and cryogenic temperature deformation of Mg-xAl-1Zn-1Ca alloy (x = 1, 2 wt.%). *J. Magnes. Alloys* **2024**, *12*, 4694–4708. [CrossRef]
70. Chaudry, U.M.; Hamad, K.; Kim, J.-G. On the ductility of magnesium based materials: A mini review. *J. Alloys Compd.* **2019**, *792*, 652–664. [CrossRef]
71. He, Y.-Y.; Lei, L.-P.; Fang, G. Interactions between dynamic recrystallization and dynamic precipitation during hot forming of magnesium alloy: Multilevel cellular automaton modeling. *J. Magnes. Alloys* **2024**. [CrossRef]
72. Mouhib, F.; Xie, Z.; Atila, A.; Guénolé, J.; Korte-Kerzel, S.; Al-Samman, T. Exploring solute behavior and texture selection in magnesium alloys at the atomistic level. *Acta Mater.* **2024**, *266*, 119677. [CrossRef]
73. Lorimer, G.W.; Mackenzie, L.W.F.; Humphreys, F.J.; Wilks, T. The recrystallization behavior of AZ31 and WE43. *Mater. Sci. Forum* **2005**, *488*, 99–102. [CrossRef]
74. Li, L.; Liu, W.; Qi, F.; Wu, D.; Zhang, Z. Effects of deformation twins on microstructure evolution, mechanical properties and corrosion behaviors in magnesium alloys—A review. *J. Magnes. Alloys* **2022**, *10*, 2334–2353. [CrossRef]
75. Zhang, K.; Zheng, J.-H.; Huang, Y.; Pruncu, C.; Jiang, J. Evolution of twinning and shear bands in magnesium alloys during rolling at room and cryogenic temperature. *Mater. Des.* **2020**, *193*, 108793. [CrossRef]
76. Mouhib, F.-Z.; Sheng, F.; Mandia, R.; Pei, R.; Korte-Kerzel, S.; Al-Samman, T. Texture Selection Mechanisms during Recrystallization and Grain Growth of a Magnesium-Erbium-Zinc Alloy. *Metals* **2021**, *11*, 171. [CrossRef]
77. Zhao, H.-D.; Qin, G.-W.; Ren, Y.-P.; Pei, W.-L.; Dong, C.; Yun, G. Microstructure and tensile properties of as-extruded Mg-Sn-Y alloys. *Trans. Nonferrous Met. Soc. China* **2010**, *20*, s493–s497. [CrossRef]
78. Ansari, N.; Sarvesha, R.; Lee, S.Y.; Singh, S.S.; Jain, J. Influence of yttrium addition on recrystallization, texture and mechanical properties of binary Mg–Y alloys. *Mater. Sci. Eng. A* **2020**, *793*, 139856. [CrossRef]
79. Zhang, J.H.; Nie, K.B.; Deng, K.K.; Han, X.Z.; Wang, Z.D. Effect of Nd on the microstructure and mechanical properties of Mg–3Zn-0.5Zr alloy. *Mater. Sci. Eng. A* **2022**, *838*, 142562. [CrossRef]
80. Mahjoub, R.; Stanford, N. The electronic origins of the "rare earth" texture effect in magnesium alloys. *Sci. Rep.* **2021**, *11*, 14159. [CrossRef] [PubMed]
81. Ding, H.; Shi, X.; Wang, Y.; Cheng, G.; Kamado, S. Texture weakening and ductility variation of Mg–2Zn alloy with CA or RE addition. *Mater. Sci. Eng. A* **2015**, *645*, 196–204. [CrossRef]
82. Chaudry, U.M.; Han, G.; Noh, Y.; Jun, T.-S. Effect of Ca alloying and cryogenic temperature on the slip transmission across the grain boundary in pure Mg. *J. Alloys Compd.* **2023**, *950*, 169828. [CrossRef]
83. Chai, Y.; Jiang, B.; Song, J.; Wang, Q.; Gao, H.; Liu, B.; Huang, G.; Zhang, D.; Pan, F. Improvement of mechanical properties and reduction of yield asymmetry of extruded Mg-Sn-Zn alloy through Ca addition. *J. Alloys Compd.* **2019**, *782*, 1076–1086. [CrossRef]
84. Song, G.; Atrens, A. Understanding Magnesium Corrosion—A Framework for Improved Alloy Performance. *Adv. Eng. Mater.* **2003**, *5*, 837–858. [CrossRef]
85. Chaudry, U.M.; Farooq, A.; Sufyan, M.; Rehan, H.M.; Tariq, A.M.; Kim, M.; Tariq, A.; Hamad, K.; Jun, T.-S. Corrosion behavior of AZ31 and AZ31-0.5 Ca in different concentrations of NaCl and $Na_2SO_4$ at various temperatures. *CORROSION* **2025**, 4620. [CrossRef] [PubMed]
86. Atrens, A.; Song, G.-L.; Liu, M.; Shi, Z.; Cao, F.; Dargusch, M.S. Review of Recent Developments in the Field of Magnesium Corrosion. *Adv. Eng. Mater.* **2015**, *17*, 400–453. [CrossRef]
87. Huo, W.T.; Lin, X.; Yu, S.; Yu, Z.T.; Zhang, W.; Zhang, Y.S. Corrosion behavior and cytocompatibility of nano-grained AZ31 Mg alloy. *J. Mater. Sci.* **2019**, *54*, 4409–4422. [CrossRef]
88. Liu, M.; Uggowitzer, P.J.; Nagasekhar, A.V.; Schmutz, P.; Easton, M.; Song, G.L.; Atrens, A. Calculated phase diagrams and the corrosion of die-cast Mg-Al alloys. *Corros. Sci.* **2009**, *51*, 602–619. [CrossRef]
89. Song, G.; Atrens, A.; Wu, X.; Zhang, B. Corrosion behaviour of AZ21, AZ501 and AZ91 in sodium chloride. *Corros. Sci.* **1998**, *40*, 1769–1791. [CrossRef]

90. Minárik, P.; Král, R.; Janeček, M. Effect of ECAP processing on corrosion resistance of AE21 and AE42 magnesium alloys. *Appl. Surf. Sci.* **2013**, *281*, 44–48. [CrossRef]
91. Gu, D.-D.; Peng, J.; Wang, J.-W.; Liu, Z.-T.; Pan, F.-S. Effect of Mn Modification on the Corrosion Susceptibility of Mg–Mn Alloys by Magnesium Scrap. *Acta Metall. Sin. (Engl. Lett.)* **2021**, *34*, 1–11. [CrossRef]
92. Xie, Q.; Ma, A.; Jiang, J.; Liu, H.; Cheng, Z.; Gu, Y. Tailoring the corrosion behavior and mechanism of AZ31 magnesium alloys by different Ca contents for marine application. *Corros. Sci.* **2021**, *192*, 109842. [CrossRef]
93. Liu, Y.; Wu, Y.; Bian, D.; Gao, S.; Leeflang, S.; Guo, H.; Zheng, Y.; Zhou, J. Study on the Mg-Li-Zn ternary alloy system with improved mechanical properties, good degradation performance and different responses to cells. *Acta Biomater.* **2017**, *62*, 418–433. [CrossRef] [PubMed]
94. Zhou, X.; Huang, Y.; Wei, Z.; Chen, Q.; Gan, F. Improvement of corrosion resistance of AZ91D magnesium alloy by holmium addition. *Corros. Sci.* **2006**, *48*, 4223–4233. [CrossRef]
95. Rosalbino, F.; Angelini, E.; De Negri, S.; Saccone, A.; Delfino, S. Electrochemical behaviour assessment of novel Mg-rich Mg-Al-RE alloys (RE = Ce, Er). *Intermetallics* **2006**, *14*, 1487–1492. [CrossRef]
96. Shi, Z.; Cao, F.; Song, G.-L.; Liu, M.; Atrens, A. Corrosion behaviour in salt spray and in 3.5% NaCl solution saturated with Mg(OH)2 of as-cast and solution heat-treated binary Mg–RE alloys: RE=Ce, La, Nd, Y, Gd. *Corros. Sci.* **2013**, *76*, 98–118. [CrossRef]
97. Trivedi, P.; Nune, K.; Misra, R. Degradation behaviour of magnesium-rare earth biomedical alloys. *Mater. Technol.* **2016**, *31*, 726–731. [CrossRef]
98. Yang, M.; Liu, X.; Zhang, Z.; Song, Y.; Bai, L. Effect of adding rare earth elements Er and Gd on the corrosion residual strength of magnesium alloy. *Open Phys.* **2019**, *17*, 373–380. [CrossRef]
99. Birbilis, N.; Easton, M.A.; Sudholz, A.D.; Zhu, S.M.; Gibson, M.A. On the corrosion of binary magnesium-rare earth alloys. *Corros. Sci.* **2009**, *51*, 683–689. [CrossRef]
100. Özarslan, S.; Şevik, H.; Sorar, İ. Microstructure, mechanical and corrosion properties of novel Mg-Sn-Ce alloys produced by high pressure die casting. *Mater. Sci. Eng. C* **2019**, *105*, 110064. [CrossRef] [PubMed]
101. Kania, A.; Nowosielski, R.; Gawlas-Mucha, A.; Babilas, R. Mechanical and Corrosion Properties of Mg-Based Alloys with Gd Addition. *Materials* **2019**, *12*, 1775. [CrossRef] [PubMed]
102. Dragomir, L.; Antoniac, I.; Manescu, V.; Antoniac, A.; Miculescu, M.; Trante, O.; Streza, A.; Cotruț, C.M.; Forna, D.A. Microstructure and Corrosion Behaviour of Mg-Ca and Mg-Zn-Ag Alloys for Biodegradable Hard Tissue Implants. *Crystals* **2023**, *13*, 1213. [CrossRef]
103. Li, J.-S.; Li, M.-X.; Hua, Z.-M.; Mo, Y.-T.; Guan, K.; Zha, M.; Gao, Y.; Wang, H.-Y. A corrosion-resistant and age-hardenable Mg-Al-Mn-Ca-Ce dilute alloy with fine-grained structure processed by controlled rolling. *J. Mater. Sci. Technol.* **2023**, *163*, 223–236. [CrossRef]
104. Sovík, J.; Hadzima, B.; Papenberg, N.P.; Arnoldt, A.R.; Gneiger, S. Investigations of Electrochemical Characteristics of Mg-Al-Ca Alloys. *Crystals* **2023**, *13*, 1684. [CrossRef]
105. Yang, P.; Ye, S.; Feng, B.; Liu, J.; Huang, S.; Liu, G.; Zhang, W.; Tang, W.; Zhu, S.; Zhang, S. Microgalvanic Corrosion of Mg–Ca and Mg–Al–Ca Alloys in NaCl and $Na_2SO_4$ Solutions. *Materials* **2021**, *14*, 7140. [CrossRef]
106. Bahmani, A.; Arthanari, S.; Shin, K.S. Corrosion behavior of Mg–Mn–Ca alloy: Influences of Al, Sn and Zn. *J. Magnes. Alloys* **2019**, *7*, 38–46. [CrossRef]
107. AbdelGawad, M.; Usman, C.A.; Shunmugasamy, V.C.; Karaman, I.; Mansoor, B. Corrosion behavior of Mg-Zn-Zr-RE alloys under physiological environment—Impact on mechanical integrity and biocompatibility. *J. Magnes. Alloys* **2022**, *10*, 1542–1572. [CrossRef]
108. Najafi, S.; Sheikhani, A.; Sabbaghian, M.; Nagy, P.; Fekete, K.; Gubicza, J. Modification of the Tensile Performance of an Extruded ZK60 Magnesium Alloy with the Addition of Rare Earth Elements. *Materials* **2023**, *16*, 2828. [CrossRef] [PubMed]
109. Nie, J.-F. Precipitation and hardening in magnesium alloys. *Metall. Mater. Trans. A* **2012**, *43*, 3891–3939. [CrossRef]
110. Peng, Q.; Wu, Y.; Fang, D.; Meng, J.; Wang, L. Microstructures and mechanical properties of Mg–8Gd–0.6 Zr–x Nd (x= 0, 1, 2 and 3 mass%) alloys. *J. Mater. Sci.* **2007**, *42*, 3908–3913. [CrossRef]
111. Peng, Q.; Wu, Y.; Fang, D.; Meng, J.; Wang, L. Microstructures and properties of Mg–7Gd alloy containing Y. *J. Alloys Compd.* **2007**, *430*, 252–256. [CrossRef]
112. Peng, Q.; Wang, J.; Wu, Y.; Wang, L. Microstructures and tensile properties of Mg–8Gd–0.6 Zr–xNd–yY (x + y = 3, mass%) alloys. *Mater. Sci. Eng. A* **2006**, *433*, 133–138. [CrossRef]
113. Peng, Q.; Dong, H.; Wang, L.; Wu, Y.; Wang, L. Microstructure and mechanical property of Mg–8.31Gd–1.12Dy–0.38Zr alloy. *Mater. Sci. Eng. A* **2008**, *477*, 193–197. [CrossRef]
114. Yamada, K.; Hoshikawa, H.; Maki, S.; Ozaki, T.; Kuroki, Y.; Kamado, S.; Kojima, Y. Enhanced age-hardening and formation of plate precipitates in Mg–Gd–Ag alloys. *Scr. Mater.* **2009**, *61*, 636–639. [CrossRef]
115. Tong, X.; Wu, G.; Easton, M.A.; Sun, M.; Wang, Q.; Zhang, L. Microstructural evolution and strengthening mechanism of Mg-Y-RE-Zr alloy fabricated by quasi-directed energy deposition. *Addit. Manuf.* **2023**, *67*, 103487. [CrossRef]

116. Shi, Q.; Natarajan, A.R.; Van der Ven, A.; Allison, J. Partitioning of Ca to metastable precipitates in a Mg-rare earth alloy. *Mater. Res. Lett.* **2023**, *11*, 222–230. [CrossRef]
117. Zhang, J.-H.; Tang, D.-X.; Zhang, H.-J.; Wang, L.-M.; Wang, J.; Meng, J. Effect and application of rare earth element in magnesium alloys. *Chin. J. Rare Met.* **2008**, *32*, 659–667.
118. Chaudry, U.M.; Tariq, H.M.R.; Ansari, N.; Kim, C.-S.; Lee, S.Y.; Jun, T.-S. Exceptional improvement in the yield strength of AZ61 magnesium alloy via cryo-stretching and its implications on the grain growth during annealing. *J. Alloys Compd.* **2024**, *970*, 172630. [CrossRef]
119. Han, G.; Noh, Y.; Chaudry, U.M.; Park, S.H.; Hamad, K.; Jun, T.-S. {10–12} extension twinning activity and compression behavior of pure Mg and Mg-0.5 Ca alloy at cryogenic temperature. *Mater. Sci. Eng. A* **2022**, *831*, 142189. [CrossRef]
120. Li, M.-Y.; Guan, Z.-P.; Liu, L.-P.; Jia, H.-J.; Li, Z.-G.; Wang, M.-H.; Ma, P.-K.; Song, J.-W. Investigation of enhanced strength anisotropy in an extruded Mg–Al–Ca–Mn alloy at cryogenic temperature. *Mater. Sci. Eng. A* **2024**, *890*, 145940. [CrossRef]
121. Hu, J.; Yang, G.; Liu, Z.; Fu, S.; Gao, H. Effects of deep cryogenic treatment on microstructure, mechanical, and corrosion of ZK60 Mg alloy. *J. Mater. Res. Technol.* **2023**, *26*, 3686–3700. [CrossRef]
122. Chen, X.; Liu, C.; Wan, Y.; Jiang, S.; Han, X.; Chen, Z. Formation of nanocrystalline AZ31B Mg alloys via cryogenic rotary swaging. *J. Magnes. Alloys* **2023**, *11*, 1580–1591. [CrossRef]
123. Zhang, K.; Zheng, J.-H.; Hopper, C.; Sun, C.; Jiang, J. Enhanced plasticity at cryogenic temperature in a magnesium alloy. *Mater. Sci. Eng. A* **2021**, *811*, 141001. [CrossRef]
124. Montana, J.; Nelson, E. *ZM-21 Magnesium Alloy Corrosion Properties and Cryogenic to Elevated Temperature Mechanical Properties*; NASA: Washington, DC, USA, 1972.
125. Fenn, R. Low-temperature properties of cast and wrought magnesium alloys. In *Symposium on Low-Temperature Properties of High-Strength Aircraft and Missile Materials*; ASTM International: West Conshohocken, PA, USA, 1961.
126. Tariq, H.M.R.; Chaudry, U.M.; Kim, C.-S.; Jun, T.-S. Synergetic improvement in strength and ductility of AZX211 Mg alloy facilitated by {10–12}-{01–12} twin-twin interactions during pre-stretching at cryogenic temperature. *J. Mater. Res. Technol.* **2024**, *29*, 3249–3254. [CrossRef]
127. Bhale, P.; Shastri, H.; Mondal, A.; Masanta, M.; Kumar, S. Effect of deep cryogenic treatment on microstructure and properties of AE42 Mg alloy. *J. Mater. Eng. Perform.* **2016**, *25*, 3590–3598. [CrossRef]
128. Tariq, H.M.R.; Kang, H.H.; Chaudry, U.M.; Khan, M.K.; Jun, T.S. Impact of Surface Roughness on the Yield Drop of Hot-Rolled AZX311 Mg Alloy. *Adv. Eng. Mater.* **2024**, 2401689. [CrossRef]
129. Zasypkin, S.; Cheretaeva, A.; Shafeev, M.; Merson, D.; Krishtal, M. Mechanical properties and corrosion resistance of Mg-RE cast alloys and their plasma electrolytic oxidation. *J. Phys. Conf. Ser.* **2021**, *2144*, 012010. [CrossRef]
130. Xu, S.; Oh-Ishi, K.; Kamado, S.; Uchida, F.; Homma, T.; Hono, K. High-strength extruded Mg–Al–Ca–Mn alloy. *Scr. Mater.* **2011**, *65*, 269–272. [CrossRef]
131. Wan, Y.; Zeng, Y.; Dou, Y.; Hu, D.; Qian, X.; Zeng, Q.; Sun, K.; Quan, G. Improved mechanical properties and strengthening mechanism with the altered precipitate orientation in magnesium alloys. *J. Magnes. Alloys* **2022**, *10*, 1256–1267. [CrossRef]
132. Nie, J.F. Effects of precipitate shape and orientation on dispersion strengthening in magnesium alloys. *Scr. Mater.* **2003**, *48*, 1009–1015. [CrossRef]
133. Li, Z.T.; Qiao, X.G.; Xu, C.; Liu, X.Q.; Kamado, S.; Zheng, M.Y. Enhanced strength by precipitate modification in wrought Mg–Al–Ca alloy with trace Mn addition. *J. Alloys Compd.* **2020**, *836*, 154689. [CrossRef]
134. Huang, Q.; Liu, Y.; Tong, M.; Pan, H.; Yang, C.; Luo, T.; Yang, Y. Enhancing tensile strength of Mg–Al–Ca wrought alloys by increasing Ca concentration. *Vacuum* **2020**, *177*, 109356. [CrossRef]
135. Wang, J.; Meng, J.; Zhang, D.; Tang, D. Effect of Y for enhanced age hardening response and mechanical properties of Mg–Gd–Y–Zr alloys. *Mater. Sci. Eng. A* **2007**, *456*, 78–84. [CrossRef]
136. Zhao, Y.; Wang, Q.D.; Gu, J.H.; Gao, Y.; Tong, Y. Microstructure and mechanical properties of Mg-Gd-Sm-Zr alloy. *Mater. Sci. Forum* **2007**, *546*, 159–162. [CrossRef]
137. Peng, Q.; Dong, H.; Wang, L.; Wu, Y.; Wang, L. Aging behavior and mechanical properties of Mg–Gd–Ho alloys. *Mater. Charact.* **2008**, *59*, 983–986. [CrossRef]
138. Fan, R.; Wang, L.; Zhao, S.; Wang, L.; Guo, E. Strengthening of Mg Alloy with Multiple RE Elements with Ag and Zn Doping via Heat Treatment. *Materials* **2023**, *16*, 4155. [CrossRef]


**Disclaimer/Publisher's Note:** The statements, opinions and data contained in all publications are solely those of the individual author(s) and contributor(s) and not of MDPI and/or the editor(s). MDPI and/or the editor(s) disclaim responsibility for any injury to people or property resulting from any ideas, methods, instructions or products referred to in the content.